doi:10.1016/j.jmb.2004.07.076 J. Mol. Biol. (2004) 342, 1337–1345

JMB

Available online at www.sciencedirect.com

SCIENCE DIRECT®

ELSEVIER

Aquaporin-0 Membrane Junctions Form Upon Proteolytic Cleavage

Tamir Gonen[1], Yifan Cheng[1], Joerg Kistler[2] and Thomas Walz[1]*

[1]*Department of Cell Biology Harvard Medical School, 240 Longwood Avenue, Boston MA 02115, USA*

[2]*School of Biological Sciences University of Auckland Auckland, PO Box 92019 New Zealand*

**Corresponding author*

Aquaporin-0 (AQP0), previously known as major intrinsic protein (MIP), is the only water pore protein expressed in lens fiber cells. AQP0 is highly specific to lens fiber cells and constitutes the most abundant intrinsic membrane protein in these cells. The protein is initially expressed as a full-length protein in young fiber cells in the lens cortex, but becomes increasingly cleaved in the lens core region. Reconstitution of AQP0 isolated from the core of sheep lenses containing a proportion of truncated protein, produced double-layered two-dimensional (2D) crystals, which displayed the same dimensions as the thin 11 nm lens fiber cell junctions, which are prominent in the lens core. In contrast reconstitution of full-length AQP0 isolated from the lens cortex reproducibly yielded single-layered 2D crystals. We present electron diffraction patterns and projection maps of both crystal types. We show that cleavage of the intracellular C terminus enhances the adhesive properties of the extracellular surface of AQP0, indicating a conformational change in the molecule. This change of function of AQP0 from a water pore in the cortex to an adhesion molecule in the lens core constitutes another manifestation of the gene sharing concept originally proposed on the basis of the dual function of crystallins.

Keywords: Aquaporin-0; AQP0; major intrinsic protein; MIP; lens junction

Introduction

Aquaporin-0 (AQP0), formerly known as major intrinsic protein (MIP), is a member of the ubiquitous aquaporin family. In contrast to most mammalian aquaporins which are expressed in more than one tissue, AQP0 is highly specific to the lens, where it is only expressed in the fiber cells. Aquaporins function as pores that are either highly selective for water (aquaporins) or are also permeable to other small neutral solutes such as glycerol (aquaglyceroporins).[1] AQP0 has been shown to conduct glycerol *in vitro*, but in the lens its function is most likely restricted to water conductance.[2]

The function of lens-specific AQP0 is intimately linked to the function of the lens. To efficiently focus incoming light onto the retina at the back of the eye, the lens has to be transparent and, depending on the distance of the observed object from the eye, the lens has to change its shape, a process referred to as accommodation. The lens has developed some remarkable adaptations to render it transparent. Differentiating lens fiber cells degrade their organelles and express a large amount of crystallins to create the correct refractive index.[3] Light scattering is further minimized by the lack of blood vessels in the lens and by the tight packing of the fiber cells, which reduces the intercellular spaces to a distance smaller than the wavelength of visible light.[3]

Lens accommodation is accompanied by significant volume changes of the fiber cells, which require water to enter and exit fiber cells very rapidly, necessitating the presence of water pores in the fiber cell membranes. AQP0 water conductance is also at the heart of the lens micro-circulation system.[3,4] Since the lens lacks blood vessels, and since passive diffusion has been shown to be insufficient, this circular flow of solutes in the lens has been proposed to supply deeper-lying fiber cells with nutrients and to clear them from waste products. This model is currently under experimental test.[5–7] In addition to rendering fiber cell

Abbreviations used: AQP0, Aquaporin-0; MIP, major intrinsic protein; AFM, atomic force microscopy; DM, decyl maltoside; LPR, lipid-to-protein ratio; DMPC, dimyristoyl phosphatidyl choline.

E-mail address of the corresponding author: twalz@hms.harvard.edu

membranes water-permeable, AQP0 also plays a structural role. It forms membrane junctions between fiber cells[8–10] and thus assists in the tight cell packing. AQP0 also provides membrane-binding sites for crystallins.[11]

AQP0 is a rather poor water pore. At neutral pH, AQP0 water permeability is approximately 40 times lower than that of AQP1.[12] AQP0 is, however, a highly abundant integral membrane protein in lens fiber cells. The vast number of water pores expressed in the plasma membrane would seem to compensate for the rather poor water conductance of individual AQP0 molecules. Furthermore, recent studies have demonstrated that AQP0 water conductance can double under mildly acidic conditions,[13] such as those found in the core of the lens.[14]

Unlike all other aquaporins, AQP0 is known to be present in single membranes as well as in membrane junctions between lens fiber cells. It is particularly enriched in the 11–13 nm thin junctions, which are abundant in the more acidic lens core and feature square AQP0 arrays.[10] The propensity of AQP0 to interact with itself has also been demonstrated by reconstitution of the protein into liposomes, which aggregated only when AQP0 was present.[15] When AQP0 was reconstituted into two-dimensional (2D) crystals, electron and atomic force microscopy (AFM) analysis revealed that these crystals were double-layered with the extracellular surfaces of the AQP0 molecules making specific interactions.[16,17] Recently, we observed that reconstitution of AQP0 purified from the lens core formed double-layered 2D crystals, and we determined the structure of such junctional AQP0 by electron crystallography.[18] The junctions formed *via* specific interactions of extracellular loops A and C, and were almost exclusively mediated by proline residues. In contrast to all other aquaporin structures, which exhibited open pores, junctional AQP0 pores were highly constricted, making the passage of water rather unlikely. It thus appears that the formation of membrane junctions converts AQP0 from a water pore to a pure membrane adhesion molecule.

The causes that induce AQP0 to form membrane junctions are yet to be identified. In the differentiation and maturation of lens fiber cells, AQP0 undergoes several post-translational modifications including deamidation and phosphorylation on its carboxyl tail.[19] As fiber cells grow older and become buried more deeply in the lens, some of the AQP0 is C-terminally cleaved at various sites in an age-dependent manner.[20,21] This process is accelerated in cataract formation.[22,23] While it has been reported that C-terminal cleavage does not affect AQP0 water conductance across the fiber cell membrane,[24] here we show that C-terminal truncation enhances the adhesive properties of the extracellular surface of AQP0 resulting in the formation of crystalline junctions in reconstitution experiments.

Results

Proteolytic cleavage causes AQP0 tetramers to pair

To study differences between full-length and truncated AQP0, we isolated membranes from the lens cortex containing full-length AQP0 (Figure 1A, lane 1) and from the lens core, which contains a mixture of full-length and truncated AQP0 (Figure 1A, lane 3). The membranes were solubilized with decyl maltoside (DM) and AQP0 purified by subsequent ion exchange and size exclusion chromatography steps. Cortical full-length AQP0 eluted from the size exclusion column almost exclusively in a single peak corresponding to a tetramer (Figure 1B, continuous line). By contrast, core AQP0 containing some truncated protein showed a second peak corresponding to a larger rather than the expected smaller molecular mass species (Figure 1B, dotted line). Since the molecular mass of this species was approximately twice the molecular mass of an AQP0 tetramer, it corresponds most likely to paired tetramers. This was supported by negative stain electron microscopy, which showed a homogeneous particle population for cortical AQP0, while core AQP0 contained a fraction of larger particles that were consistent in size and shape with two stacked AQP0 tetramers (data not shown). Next, we treated purified DM-solubilized AQP0 with chymotrypsin, which reduced the molecular mass of AQP0 from 26 kDa to 22 kDa (Figure 1A, lane 2). Analysis of the chymotrypsin-treated AQP0 by size exclusion chromatography (Figure 1B, broken line) revealed that almost all the AQP0 tetramers were now paired.

Analysis of the C and N-terminal truncations of AQP0

We have previously determined the amino acid sequence of full-length sheep AQP0[18] and the

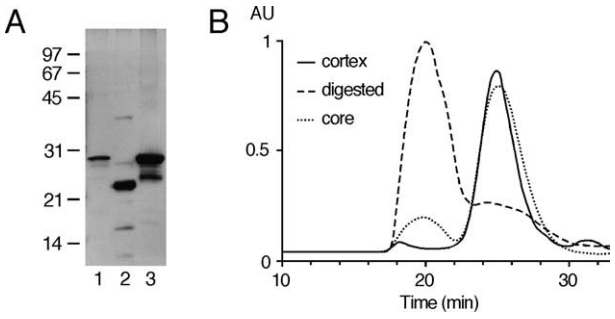

Figure 1. Cleavage of AQP0 results in tetramer pairing. A, Silver stained SDS-12% PAGE of AQP0 isolated from the lens cortex before (lane 1) and after treatment with chymotrypsin (lane 2) and AQP0 isolated from the lens core containing a mixture of full-length and cleaved AQP0 (lane 3). B, Gel filtration elution profiles of lens cortical (continuous line), lens core (dotted line) and chymotrypsin-treated AQP0 (broken line).

primary structure is shown in Figure 2A. To characterize various cleavages of AQP0 we employed N- and C-terminal protein sequencing as well as mass spectrometry. The N terminus of *in vivo* cleaved AQP0 from the lens core is not modified (Figure 2B). Several C-terminal cleavage sites have recently been characterized by mass spectrometry[19,24] (arrows 3 and 4 in Figure 2A indicate two of the major cleavage sites in the aging lens; Figure 2B). Chymotrypsin treatment of AQP0 results in the removal of two residues from the N terminus (arrow 1 in Figure 2A and B) and 44 residues from the C terminus (arrow 2 in Figure 2A, C and B), thus eliminating the entire cytoplasmic C-terminal tail of AQP0.

Reconstitution of core AQP0 yields clustered vesicles

In vivo truncated as well as chymotrypsin-treated AQP0 showed a pronounced tendency to form paired tetramers. This finding in combination with the previous observation that AQP0-containing 11–13 nm thin junctions are predominant in the lens core,[10] where a fraction of AQP0 is cleaved, prompted us to test whether it is in fact proteolytic cleavage that gives AQP0 the ability to form membrane junctions.

Purified full-length AQP0 from the lens cortex was reconstituted into artificial bilayers by slow removal of DM in the presence of synthetic lipid (dimyristoyl phosphatidyl choline; DMPC). At a lipid-to-protein ratio (LPR) of 0.1 (w/w), small vesicles formed containing full-length AQP0 (Figure 3D, lane 1). When imaged by negative stain electron microscopy, the vesicles were evenly distributed on the carbon support film (Figure 3A). Reconstitution of core AQP0 using the same conditions yielded vesicles containing both full-length and truncated AQP0 (Figure 3D, lane 3). In this case negative stain electron microscopy showed that the resulting vesicles were not evenly dispersed on the carbon film but formed large clusters (Figure 3C). Finally, we incubated the vesicles containing full-length AQP0 (Figure 3A) with chymotrypsin, resulting in the cleavage of approximately 50% of the reconstituted AQP0 (Figure 3A, lane 2). The protease digestion was incomplete, because only broken vesicles allowed the protease access to the AQP0 C termini located in the lumen of the vesicles. Electron microscopy of the chymotrypsin-treated vesicles showed that the majority of the vesicles had aggregated into large clusters (Figure 3B).

Structural characterization of reconstituted AQP0

When full-length AQP0 was reconstituted at an LPR of 0.25, large (~2 μm in diameter) crystalline sheets formed (Figure 4A). Image processing of glucose-embedded crystals revealed a unit cell with lattice parameters of $a=b=65.5$ Å and $p4$ symmetry (Table 1). The projection map of the AQP0 tetramer at 4 Å resolution (Figure 4D; Table 2) is virtually identical with a 3.5 Å projection structure of AQP1,[25] demonstrating that 2D crystals formed by full-length AQP0 isolated from the lens cortex are single-layered.

The same reconstitution was performed using AQP0 isolated from the lens core, containing a mixture of full-length and truncated AQP0. In this case large membrane sheets formed (>6 μm) that in some cases showed two parallel edges, revealing

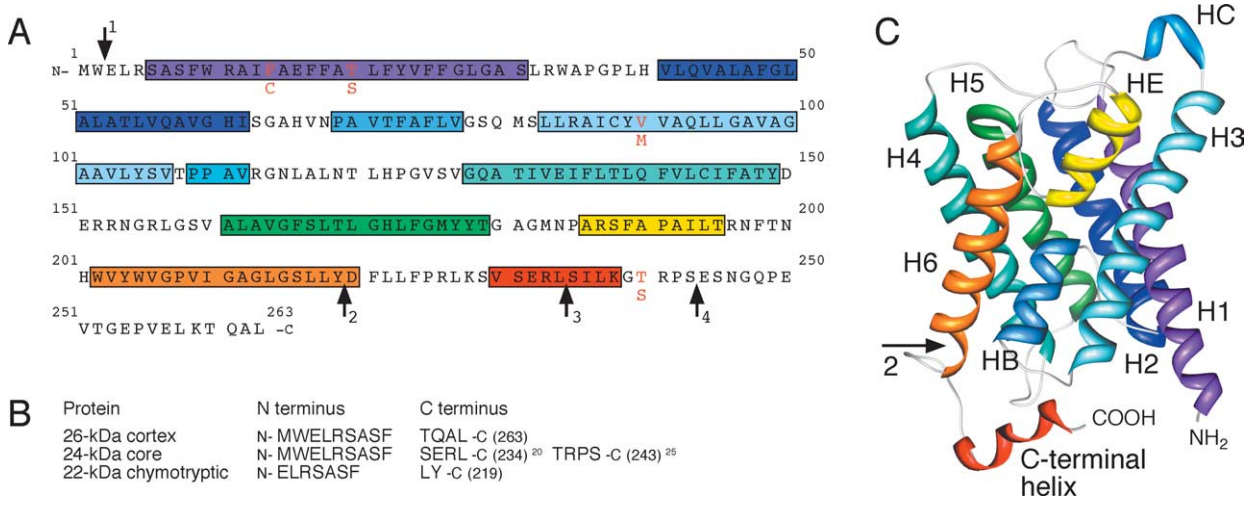

Figure 2. Sequence of sheep lens AQP0 and cleavage sites. A, Amino acid sequence of sheep lens AQP0 (GenBank accession number AY573927). The four substitutions compared to bovine AQP0 are marked by red letters. α-Helical regions are indicated by colored boxes. Arrows 1 and 2 indicate the chymotrypsin cleavage sites, while arrows 3 and 4 indicate the major *in vivo* cleavage sites in the aging lens. B, N and C termini of full-length, *in vivo* cleaved and chymotrypsin-treated AQP0. C, Ribbon diagram of full-length AQP0 with α-helical regions annotated and shown in the same colors as in A. Arrow 2 refers to the cleavage site shown in A, illustrating the complete removal of the AQP0 C terminus by chymotrypsin.

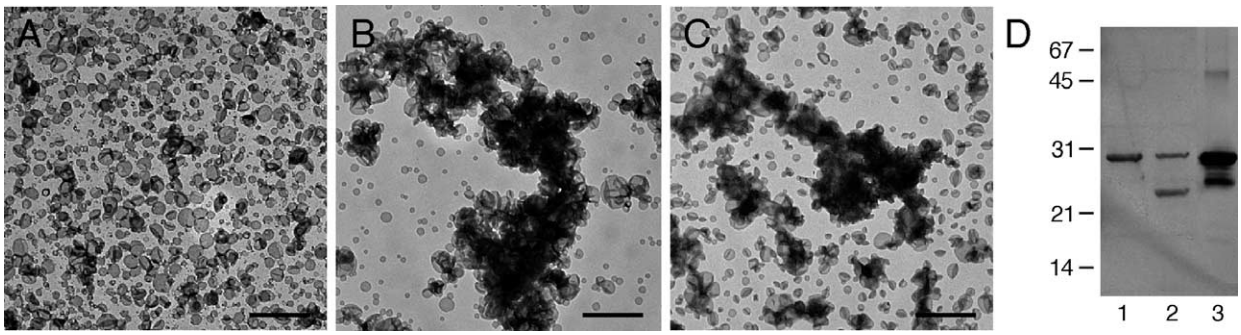

Figure 3. Cleavage of AQP0 increases its adhesive properties. A, Negative stain electron microscopy shows that reconstitution of full-length lens cortical AQP0 at an LPR of 0.1 yields small vesicles that are evenly distributed on the carbon film. B, Incubation of the vesicles shown in A with chymotrypsin causes vesicle clustering similar to the result seen in C. C, Reconstitution of AQP0 from the lens core using the same conditions that produced the dispersed vesicles shown in A, produces vesicle that are aggregated. D, Silver stained SDS-12% PAGE; lane 1: reconstituted cortical full-length AQP0; lane 2: reconstituted full-length AQP0 after chymotrypsin treatment; lane 3: reconstituted AQP0 from the lens core. Scale bars in A, B and C represent to 1 μm.

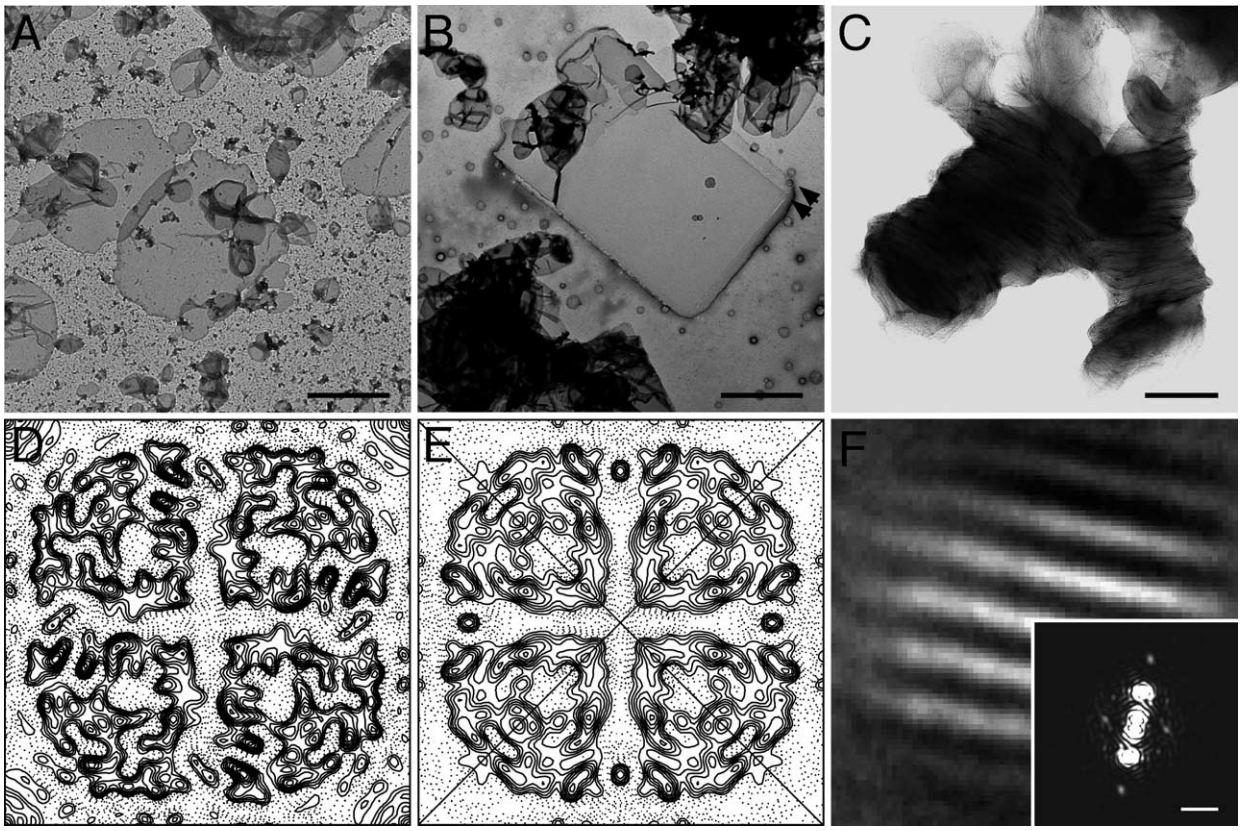

Figure 4. 2D crystallization of lens cortical and lens core AQP0. A, Reconstitution of full-length AQP0 at an LPR of 0.25 yielded large single-layered 2D crystals. B, Lens core AQP0 using the same reconstitution conditions produced large double-layered 2D crystals. The edges of the two layers can clearly be seen at the top right edge of the membrane sheet (indicated by arrowheads). C, Digestion of AQP0 prior to reconstitution resulted in large membrane stacks. D, A 4 Å projection map obtained from 11 images of glucose-embedded single-layered AQP0 crystals reveals the AQP0 tetramer. E, A 4 Å projection map obtained from nine images of double-layered AQP0 crystals reveals two mirror axes (indicated by diagonal black lines) due to the opposite orientations of the two interacting crystal layers. F, Patch average calculated from 213 areas showing the tightly packed membranes. The inset shows the calculated power spectrum revealing second order diffraction spots and a spacing between the membranes of 5.5 nm. The scale bars represent 1 μm in A and B, 0.5 μm in C, and $(5\ \text{nm})^{-1}$ in the inset of F. D and E Complete unit cells with lattice constants of $a=b=65.5$ Å. Panel F has a side length of 32.5 nm.

Table 1. Internal phase residuals of all possible two-sided plane groups of representative untilted images of a single-layered and a double-layered AQP0 2D crystal

Two-sided plane group	Single-layered crystal			Double-layered crystal		
	Phase residual[a]	Number of comparisons	Target residual[b]	Phase residual[a]	Number of comparisons	Target residual[b]
*p*1	14.3[c]	86		11.1[c]	94	
*p*2	17.1[d]	43	20.4	20.9	47	15.8
*p*12_a	30.8	33	15.2	17.8	41	11.7
*p*12_b	29.0	32	15.0	15.8[e]	41	11.7
$p12_1$_a	68.5	33	15.2	82.8	41	11.7
$p12_1$_b	65.8	32	15.0	83.8	41	11.7
*c*12_a	30.8	33	15.2	17.8	41	11.7
*c*12_b	29.0	32	15.0	15.8[e]	41	11.7
*p*222	25.3	108	16.7	18.3	129	12.8
$p222_1$_a	65.9	108	16.7	64.5	129	12.8
$p222_1$_b	66.2	108	16.7	61.4	129	12.8
$p22_12_1$	47.4	108	16.7	69.3	129	12.8
*c*222	25.3	108	16.7	18.3	129	12.8
*p*4	10.6[d]	123	16.4	17.1[e]	139	12.7
*p*422	21.2	255	15.3	15.9[e]	310	11.8
$p42_12$	42.7	255	15.3	61.9	310	11.8

Internal phase residuals were determined from spots of IQ1 to IQ5 to 12 Å resolution.
[a] Phase residual *versus* other spots (90° random).
[b] Target residual based on statistics taking Friedel weight into account.
[c] Note that in space group *p*1 no phase comparison is possible; the numbers given here are theoretical phase residuals based on the signal-to-noise ratio of the observed diffraction spots.
[d] Within 20% of target residual.
[e] Within 30% of target residual.

them to be double-layered (Figure 4B). These double-layered crystals had the same lattice constants as those observed in single-layered crystals reconstituted from cortical full-length AQP0 ($a = b = 65.5$ Å), but now had a *p*422 symmetry (Table 1). A 4 Å projection map calculated from the double-layered crystals showed a tetrameric structure with the same dimensions as an AQP0 tetramer, but each "monomer" now displaying two-fold mirror symmetry (Figure 4E; Table 2).

When AQP0 that was completely cleaved by chymotrypsin treatment was used for reconstitution, large membrane stacks formed (Figure 4C). An average of these stacked membranes was calculated from 213 patches (Figure 4F) and a power spectrum calculated from this average revealed diffraction spots corresponding to a spacing of the membranes of about 5.5 nm (Figure 4F, inset). Hence, two interacting membranes would have an overall thickness of 11 nm.

The reconstitution of single-layered crystals from cortical AQP0 and of double-layered crystals from core AQP0 was corroborated by electron diffraction analysis. Since single-layered crystals contain half as many proteins per unit area than double-layered crystals, electron diffraction patterns recorded from single-layered crystals consistently showed weaker diffraction spots than those recorded from double-layered crystals. Furthermore, whereas single-layered crystals reproducibly gave rise to diffraction patterns displaying a handedness (Figure 5A), double-layered 2D crystals always produced mirror-symmetric diffraction patterns

Table 2. Phase residuals in resolution shells

Resolution shell (Å)	Number of phases	Mean value of $\Delta\alpha_c$ (deg.)	Standard error (deg.)	Mean figure of merit
Single-layered AQP0 2D crystals (11 images, p4 symmetry)				
∞–4.0	229	13.1	1.1	0.92
∞–10.0	36	6.9	1.7	0.98
10.0–7.0	37	6.1	1.2	0.98
7.0–5.0	75	13.5	2.0	0.92
5.0–4.0	81	18.6	2.0	0.87
Double-layered AQP0 2D crystals (nine images, p422 symmetry)				
∞–4.0	129	23.8	1.9	0.85
∞–10.0	23	9.8	2.5	0.97
10.0–7.0	21	17.4	3.9	0.91
7.0–5.0	41	26.5	3.8	0.82
5.0–4.0	44	31.7	3.2	0.79

$\Delta\alpha_c$: difference between the symmetry-imposed phase of 0° and 180° and the observed combined phase. 45 degree is random.

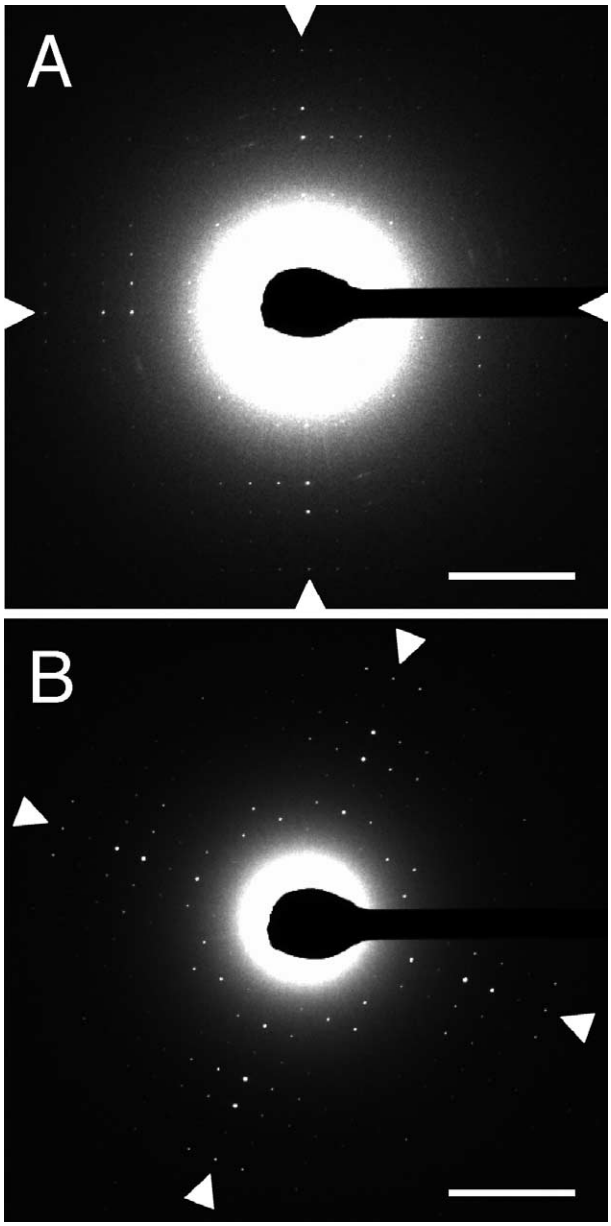

Figure 5. Electron diffraction analysis of single- and double-layered AQP0 2D crystals. A, The electron diffraction pattern of an untilted single-layered AQP0 2D crystal shows a windmill-like pattern with a clear handedness. B, In contrast, the electron diffraction pattern of an untilted double-layered AQP0 2D crystal shows mirror symmetry and no handedness. The mirror axes, missing in A and present in B, are indicated by arrowheads. The scale bars represent to $(15\ \text{Å})^{-1}$.

consistent with the inverted orientation of the two adjoining crystalline membranes (Figure 5B).

Discussion

AQP0, at that time known as MIP, was initially thought to be a gap junction protein as it was localized to membrane junctions in the lens.[26–28] Later is was shown, however, that AQP0 was not a gap junction protein.[29,30] Once the homologous protein AQP1 was found to be a water pore,[31] interest in AQP0 shifted towards its water permeation properties.[12,13,32] The interest in AQP0 as a junctional protein has recently been rekindled when it was demonstrated that reconstitution of purified AQP0 resulted in double-layered 2D crystals.[17] We have recently been able to use such crystals to produce an atomic model for junctional AQP0 by electron crystallography.[18] AQP0, unlike most other aquaporins, is not glycosylated and features a shortened extracellular loop A between the first two membrane-spanning α-helices. These two adaptations allow AQP0 tetramers in adjoining membranes to make specific interactions, which are almost exclusively mediated by proline residues.[18]

The double-layered AQP0 2D crystals have lattice parameters of $a=b=65.5$ Å and a thickness of about 11 nm, the same dimensions as thin junctions between lens fiber cells.[9] Two types of thin junctions have been described in the literature: straight junctions that contain AQP0 in both opposing membranes[8] and wavy junctions, in which AQP0 is apparent in square arrays, which alternate regularly between the undulating junctional membranes.[10] Given the very specific proline-mediated contacts between the extracellular surfaces of AQP0 tetramers in the reconstituted crystalline junctions, we consider it unlikely that in the wavy junctions a crystalline AQP0 array interacts with an empty membrane as was proposed earlier.[10] Instead, it appears more likely that the "empty" membrane contained AQP0, which remained undetected but was available for junction formation.

The appearance of AQP0 junctions is more pronounced deeper in the lens where an increasing proportion of AQP0 has undergone age-related cleavage at the C terminus.[19] Reconstitution of AQP0 from the lens core reproducibly yielded double-layered 2D crystals, whereas full-length AQP0 from the lens cortex always produced single-layered crystals. Furthermore, vesicle clustering was only observed when proteoliposomes containing reconstituted full-length AQP0 were treated with chymotrypsin. Finally, when chymotrypsin-digested AQP0 was reconstituted, very large membrane stacks formed. All these observations are consistent with the notion that cytoplasmic cleavage enhances the adhesive properties of AQP0. Analysis of the N terminus showed that it remained intact in core AQP0. Chymotrypsin treatment only removed two residues, making it appear more likely that increased adhesion is due to the removal of the C terminus. At this point we cannot be sure, however, whether junction formation *in vivo* is the direct result of C-terminal cleavage or whether it is an indirect effect due to the removal of post-translational modifications in core AQP0, such as the well-characterized phosphorylations and deamidations of the C terminus.[19] Whichever is the case, the molecules must undergo

a conformational change as the C terminus is cytoplasmic and an increase in adhesiveness involves the extracellular surface.

The recently determined structure of junctional AQP0 showed the water pore in a closed conformation.[18] C-terminal cleavage of AQP0 alone is unlikely to be responsible for the closed pore conformation, because it had been shown previously not to affect water conductance.[24] Therefore, junction formation between opposing AQP0 tetramers is the most likely cause for the closure of the water pore. A proportion of open AQP0 water pores would, however, seem to be important for volume changes in lens fiber cells during accommodation, and to support the lens micro-circulation system.[3,4] We envisage the situation in the lens core as follows: AQP0 is a highly abundant membrane protein in lens fiber cells and only a fraction is being cleaved in the lens core. Therefore, sufficient AQP0 molecules may retain their function as water pores. Furthermore, water conductance by AQP0 is pH-dependent and is maximal at a pH around 6.5.[13] Since the lens has a pH gradient with a pH of 7.2 in the cortex and 6.5 in the core,[14] AQP0 molecules in the lens core are about twice as efficient water pores as AQP0 molecules in the cortex, offsetting the loss of a fraction of AQP0 water pores to membrane junctions. Finally, unlike in the lens cortex, connexins in the lens core are C-terminally cleaved,[33] rendering gap junctions constitutively open. Since gap junctions thus provide a large number of cell-to-cell connections, specific cell-to-cell water pores mediated by AQP0 would not appear essential in the lens core.

The closed pore conformation of junctional AQP0 strengthens an emerging view that AQP0 can serve two totally different functions: either as a water pore or as a cell adhesion protein. In the cortex, where AQP0 is present mostly as a full-length protein, it predominantly functions as a water pore, thereby playing a key role in the lens circulation system.[3,4] In the lens core, the propensity to form membrane junctions increases, thereby supporting the tight packing of fiber cells that is characteristic for the lens core. The dual function of AQP0 is consistent with the "gene sharing" concept developed previously for the lens crystallins, which were demonstrated to be functional enzymes but appear to have been recruited by the lens for predominantly structural and refractory purposes.[34] It would appear that the lens has adopted a highly efficient model of evolution, where the utilisation of protein resources is maximized.

Materials and Methods

Sequence of sheep lens AQP0

Sheep AQP0 was sequenced as described.[18] For amino acid sequencing, AQP0 was isolated from lens fiber cells and further purified by SDS-gel electrophoresis. The protein bands corresponding to full length AQP0, *in vivo* cleaved AQP0, and chymotrypsin-treated AQP0 were cut out of the gel and sent for N and C-terminal sequencing to the Macromolecular Structure Facility at Michigan State University.

Purification of AQP0

Lenses were dissected to separate the soft cortical tissue from the hard core. Depending on the experiment, membranes were prepared as described,[35] either from the lens cortex or the lens core. Membranes were solubilized with 1% (w/v) decyl maltoside (DM) in 10 mM Tris (pH 8) for 30 minutes at 37 °C, and insoluble material removed by centrifugation at 110,000*g* for 30 minutes. Proteins were bound to a MonoQ column (Amersham) equilibrated with 0.3% DM in 10 mM Tris (pH 8), and AQP0 eluted with 200 mM NaCl. For cleavage experiments, 0.2 mM α-chymotrypsin was added to purified AQP0 and incubated at 37 °C for 30 minutes. The reaction was stopped by the addition of 2 mM PMSF. Pooled fractions were run over a Superose 12 column (Amersham) pre-equilibrated with 0.3% DM in 10 mM Tris (pH 8) 150 mM NaCl. The column was calibrated using ovalbumin (45 kDa), bovine serum albumin (66 kDa), aldolase (158 kDa), thyroglobulin (670 kDa) as molecular mass marker proteins and blue dextran (2 MDa) for determination of the void column volume.

Reconstitution of purified lens AQP0 into lipid bilayers

Purified AQP0 was mixed with DM-solubilized dimyristoyl phosphatidyl choline (DMPC) at varying LPRs. The mixture was placed in a dialysis button and the detergent removed by dialysis against 10 mM Mes (pH 6), 50 mM $MgCl_2$, 150 mM NaCl, 5 mM DTT, 0.02% (w/v) NaN_3 at room temperature. For cleavage experiments, 0.2 mM α-chymotrypsin was added to half of the sample of reconstituted vesicles containing full-length cortical AQP0. To the second half, and equivalent amount of buffer was added. Both halves were incubated at 37 °C for 30 minutes and the reaction was stopped by the addition of 2 mM PMSF.

Electron microscopy and image processing

Negatively stained samples, prepared and imaged as described,[36] were used to assess the outcome of reconstitution experiments. For cryo-electron microscopy, 2D crystallization samples were mixed with an equal amount of 20% (w/v) glucose and the suspension applied to molybdenum grids (kindly provided by Dr Yoshinori Fujiyoshi) covered with a thin layer of carbon film. Grids were blotted to remove excess material, loaded onto a high-tilt cryo-transfer holder (Gatan) and transferred into a FEI Tecnai F20 electron microscope equipped with a field emission electron source and operated at 200 kV. The sample was cooled to liquid nitrogen temperature, and images were recorded under low dose conditions (<20 electrons $Å^{-2}$) at a magnification of 50,000× on Kodak SO163 film. Micrographs of well ordered crystals were selected by optical diffraction and areas of up to 10,000×10,000 pixels were digitized with a Zeiss SCAI scanner using a step size of 7 μm. Images were processed with the MRC programs[37] following established protocols.[38] In the case of single-layered 2D crystals, a *p*4 symmetry was applied and in the case of double-layered crystals a *p*422 symmetry. In either case a *B*-factor of -500 was applied to the final projection map to sharpen the

high-resolution features. Low-dose electron diffraction data were recorded with a Gatan 2 K×2 K slow-scan CCD camera using a camera length of 3000 mm and a selected area aperture of 70 μm.

Acknowledgements

This work was supported by NIH grant EY015107 (to T.W.). The EM facility at Harvard Medical School was established by a donation from the Giovanni Armenise Harvard Center for Structural Biology and is maintained by funds from NIH grant GM62580.

References

1. Agre, P., King, L. S., Yasui, M., Guggino, W. B., Ottersen, O. P., Fujiyoshi, Y. *et al*. (2002). Aquaporin water channels—from atomic structure to clinical medicine. *J. Physiol.* **542**, 3–16.
2. Varadaraj, K., Kushmerick, C., Baldo, G. J., Bassnett, S., Shiels, A. & Mathias, R. T. (1999). The role of MIP in lens fiber cell membrane transport. *J. Membr. Biol.* **170**, 191–203.
3. Donaldson, P., Kistler, J. & Mathias, R. T. (2001). Molecular solutions to mammalian lens transparency. *News Physiol. Sci.* **16**, 118–123.
4. Mathias, R. T., Rae, J. L. & Baldo, G. J. (1997). Physiological properties of the normal lens. *Physiol. Rev.* **77**, 21–50.
5. Sweeney, M. H. & Truscott, R. J. (1998). An impediment to glutathione diffusion in older normal human lenses: a possible precondition for nuclear cataract. *Expt. Eye Res.* **67**, 587–595.
6. Moffat, B. A., Landman, K. A., Truscott, R. J., Sweeney, M. H. & Pope, J. M. (1999). Age-related changes in the kinetics of water transport in normal human lenses. *Expt. Eye Res.* **69**, 663–669.
7. Moffat, B. A. & Pope, J. M. (2002). Anisotropic water transport in the human eye lens studied by diffusion tensor NMR micro-imaging. *Expt. Eye Res.* **74**, 677–687.
8. Bok, D., Dockstader, J. & Horwitz, J. (1982). Immunocytochemical localization of the lens main intrinsic polypeptide (MIP26) in communicating junctions. *J. Cell Biol.* **92**, 213–220.
9. Zampighi, G., Simon, S. A., Robertson, J. D., McIntosh, T. J. & Costello, M. J. (1982). On the structural organization of isolated bovine lens fiber junctions. *J. Cell Biol.* **93**, 175–189.
10. Costello, M. J., McIntosh, T. J. & Robertson, J. D. (1989). Distribution of gap junctions and square array junctions in the mammalian lens. *Invest. Ophthalmol. Vis. Sci.* **30**, 975–989.
11. Fan, J., Donovan, A. K., Ledee, D. R., Zelenka, P. S., Fariss, R. N. & Chepelinsky, A. B. (2004). GammaE-crystallin recruitment to the plasma membrane by specific interaction between lens MIP/aquaporin-0 and gammaE-crystallin. *Invest. Ophthalmol. Vis. Sci.* **45**, 863–871.
12. Chandy, G., Zampighi, G. A., Kreman, M. & Hall, J. E. (1997). Comparison of the water transporting properties of MIP and AQP1. *J. Membr. Biol.* **159**, 29–39.
13. Nemeth-Cahalan, K. L. & Hall, J. E. (2000). pH and calcium regulate the water permeability of aquaporin 0. *J. Biol. Chem.* **275**, 6777–6782.
14. Mathias, R. T., Riquelme, G. & Rae, J. L. (1991). Cell to cell communication and pH in the frog lens. *J. Gen. Physiol.* **98**, 1085–1103.
15. Dunia, I., Manenti, S., Rousselet, A. & Benedetti, E. L. (1987). Electron microscopic observations of reconstituted proteoliposomes with the purified major intrinsic membrane protein of eye lens fibers. *J. Cell Biol.* **105**, 1679–1689.
16. Hasler, L., Walz, T., Tittmann, P., Gross, H., Kistler, J. & Engel, A. (1998). Purified lens major intrinsic protein (MIP) forms highly ordered tetragonal two-dimensional arrays by reconstitution. *J. Mol. Biol.* **279**, 855–864.
17. Fotiadis, D., Hasler, L., Muller, D. J., Stahlberg, H., Kistler, J. & Engel, A. (2000). Surface tongue-and-groove contours on lens MIP facilitate cell-to-cell adherence. *J. Mol. Biol.* **300**, 779–789.
18. Gonen, T., Sliz, P., Kistler, J., Cheng, Y. & Walz, T. (2004). Aquaporin-0 membrane junctions reveal the structure of a closed water pore. *Nature*, **429**, 193–197.
19. Schey, K. L., Little, M., Fowler, J. G. & Crouch, R. K. (2000). Characterization of human lens major intrinsic protein structure. *Invest. Ophthalmol. Vis. Sci.* **41**, 175–182.
20. Roy, D., Spector, A. & Farnsworth, P. N. (1979). Human lens membrane: comparison of major intrinsic polypeptides from young and old lenses isolated by a new methodology. *Expt. Eye Res.* **28**, 353–358.
21. Takemoto, L., Takehana, M. & Horwitz, J. (1986). Covalent changes in MIP26K during aging of the human lens membrane. *Invest. Ophthalmol. Vis. Sci.* **27**, 443–446.
22. Takemoto, L. & Takehana, M. (1986). Covalent change of major intrinsic polypeptide (MIP26K) of lens membrane during human senile cataractogenesis. *Biochem. Biophys. Res. Commun.* **135**, 965–971.
23. Takemoto, L., Smith, J. & Kodama, T. (1987). Major intrinsic polypeptide (MIP26K) of the lens membrane: covalent change in an internal sequence during human senile cataractogenesis. *Biochem. Biophys. Res. Commun.* **142**, 761–766.
24. Ball, L. E., Little, M., Nowak, M. W., Garland, D. L., Crouch, R. K. & Schey, K. L. (2003). Water permeability of C-terminally truncated aquaporin 0 (AQP0 1-243) observed in the aging human lens. *Invest. Ophthalmol. Vis. Sci.* **44**, 4820–4828.
25. Walz, T. & Grigorieff, N. (1998). Electron crystallography of two-dimensional crystals of membrane proteins. *J. Struct. Biol.* **121**, 142–161.
26. Benedetti, E. L., Dunia, I., Bentzel, C. J., Vermorken, A. J., Kibbelaar, M. & Bloemendal, H. (1976). A portrait of plasma membrane specializations in eye lens epithelium and fibers. *Biochim. Biophys. Acta*, **457**, 353–384.
27. Broekhuyse, R. M., Kuhlmann, E. D., Bijvelt, J., Verkleij, A. J. & Ververgaert, P. H. (1978). Lens membranes III. Freeze fracture morphology and composition of bovine lens fibre membranes in relation to ageing. *Expt. Eye Res.* **26**, 147–156.
28. Goodenough, D. A. (1979). Lens gap junctions: a structural hypothesis for nonregulated low-resistance intercellular pathways. *Invest. Ophthalmol. Vis. Sci.* **18**, 1104–1122.
29. Kistler, J. & Bullivant, S. (1980). Lens gap junctions and orthogonal arrays are unrelated. *FEBS Letters*, **111**, 73–78.

30. Kistler, J., Christie, D. & Bullivant, S. (1988). Homologies between gap junction proteins in lens, heart and liver. *Nature*, **331**, 721–723.
31. Preston, G. M., Carroll, T. P., Guggino, W. B. & Agre, P. (1992). Appearance of water channels in *Xenopus* oocytes expressing red cell CHIP28 protein. *Science*, **256**, 385–387.
32. Mulders, S. M., Preston, G. M., Deen, P. M., Guggino, W. B., van Os, C. H. & Agre, P. (1995). Water channel properties of major intrinsic protein of lens. *J. Biol. Chem.* **270**, 9010–9016.
33. Lin, J. S., Eckert, R., Kistler, J. & Donaldson, P. (1998). Spatial differences in gap junction gating in the lens are a consequence of connexin cleavage. *Eur. J. Cell Biol.* **76**, 246–250.
34. Piatigorsky, J. & Wistow, G. J. (1989). Enzyme/crystallins: gene sharing as an evolutionary strategy. *Cell*, **57**, 197–199.
35. Gonen, T., Donaldson, P. & Kistler, J. (2000). Galectin-3 is associated with the plasma membrane of lens fiber cells. *Invest. Ophthalmol. Vis. Sci.* **41**, 199–203.
36. Ohi, M., Li, Y., Cheng, Y. & Walz, T. (2004). Negative staining and image classification—powerful tools in modern electron microscopy. *Biol. Proc. Online*, **6**, 23–34.
37. Crowther, R. A., Henderson, R. & Smith, J. M. (1996). MRC image processing programs. *J. Struct. Biol.* **116**, 9–16.
38. Amos, L. A., Henderson, R. & Unwin, P. N. T. (1982). Three-dimensional structure determination by electron microscopy of two-dimensional crystals. *Prog. Biophys. Mol. Biol.* **39**, 183–231.

Edited by W. Baumeister

(Received 25 March 2004; received in revised form 8 July 2004; accepted 15 July 2004)